DOE/NASA/20320-41
NASA TM-82944



# Theoretical and Experimental Power From Large Horizontal-Axis Wind Turbines


Larry A. Viterna and David C. Janetzke
National Aeronautics and Space Administration
Lewis Research Center

**September 1982**

Prepared for
**U.S. DEPARTMENT OF ENERGY**
**Conservation and Renewable Energy**
**Wind Energy Technology Division**

DOE/NASA/20320-41
NASA TM-82944

# Theoretical and Experimental Power From Large Horizontal-Axis Wind Turbines

Larry A. Viterna and David C. Janetzke
National Aeronautics and Space Administration
Lewis Research Center
Cleveland, Ohio 44135

September 1982

Work performed for
U.S. DEPARTMENT OF ENERGY
Conservation and Renewable Energy
Wind Energy Technology Division
Washington, D.C. 20545
Under Interagency Agreement DE-AI01-76ET20320

# THEORETICAL AND EXPERIMENTAL POWER FROM LARGE HORIZONTAL-AXIS WIND TURBINES*

Larry A. Viterna and David C. Janetzke

National Aeronautics and Space Administration
Lewis Research Center
Cleveland, Ohio



## SUMMARY

A method for calculating the output power from large horizontal-axis wind turbines is presented. Modifications to the airfoil characteristics and the momentum portion of classical blade element-momentum theory are given that improve correlation with measured data. Improvement is particularly evident at low tip speed ratios where aerodynamic stall can occur as the blade experiences high angles of attack.

Output power calculated using the modified theory is compared with measured data for several large wind turbines. These wind turbines range in size from the DOE/NASA 100 kW Mod-0 (38 m rotor diameter) to the 2000 kW Mod-1 (61 m rotor diameter). The calculated results are in good agreement with measured data from these machines.

## INTRODUCTION

To correctly assess the cost of energy of the next generation of wind turbines, a validated method of predicting aerodynamic performance is required. Several methods have been available (refs. 1 and 2), however, the results from which have not been sufficiently verified with experimental data from a variety of operating wind turbines.

Classical blade element-momentum theory has been found to give adequate results under normal operating conditions near the design tip-speed ratio (ratio of blade tip speed to wind speed). At both high and low tip-speed ratios, however, the wind turbine may operate in flow conditions which are not easily analyzed by classical theory. Recent tests on the NASA Mod-0 100 kW wind turbine, for example, indicate that classical theory is inadequate at low tip-speed ratios when the airfoils are at high angles of attack. This problem can be particularly important in the calculation of fixed-pitch and tip-control rotor performance. Since the maximum power produced by a fixed pitch rotor is a critical design parameter, efforts are being made to improve theoretical analysis of this operating condition. At high tip-speed ratios, the rotor may operate in the vortex ring state in which a vortex ring is formed in the rotor plane. Under this condition an eddy motion occurs, such as behind a bluff body, and the overall thrust force on the rotor can deviate significantly

*Based on a presentation given at the Fifth Biennial Conference and Workshop on Wind Energy, October 5-7, 1981. SERI/CP-635-1340, DOE Publication CONF-811043, vol. 2.

from values given by momentum theory (ref. 3). Furthermore, from a practical viewpoint, analysis of this state using momentum theory can cause difficult convergence problems and result in unrealistic values in the calculation of the induced flow velocities.

Experimental data from two Mod-0 rotor configurations as well as from the Mod-0A and Mod-1 wind turbines were analyzed. Empirical corrections to both the airfoil characteristics and momentum theory are presented which improve the correlation with experimental results. Improvement is most noticeable in the power output versus wind speed at low tip speed ratios.

## CLASSICAL THEORY

Blade element-momentum theory used in the PROP Code (ref. 1), as well as others, divides the blade into small spanwise elements. These elements are considered to act as airfoil segments in two-dimensional flow fields, each at a particular angle of attack. The effects of tower shadow and nonuniform inflow have been found to be small and are generally neglected. From the geometry, the rotational velocity component, the wind component, and the "induced" axial and rotational components, the local angle of attack is calculated. The lift and drag forces on the elements are then determined from two-dimensional (infinite aspect ratio) wind tunnel data at the local angle of attack (ref. 4). Comparison of cambered and uncambered data indicates little difference in airfoil performance beyond stall; therefore, data for symmetric sections may be used for this region (ref. 5). The "induced effects" of the wind turbine on the flow are determined in an iterative procedure until momentum considerations are satisfied. The end effects of the finite-length wind turbine blade are included by using a tip loss model. There are a variety of these tip-loss models, the simplest being to reduce the lift coefficient to zero for approximately 3 percent of the radius near the tips. A more complete description of blade element-momentum theory is contained in reference 1.

## LOW TIP SPEED RATIO OPERATION

Tests were run on the NASA Mod-0 100 kW wind turbine to investigate the performance characteristics of fixed-pitch rotors at low tip-speed ratios (high winds). Under this condition, the airfoils operate at high angles of attack and aerodynamic stall can occur.

### Test Configurations and Operating Conditions

Two rotors were used in the Mod-0 tests, both of which were 38 m in diameter. Details of the blade planform, twist, etc. are given in tables I(a) and (b) and figures 1(a) and (b). The significant differences between the two blades are that the aluminum blades have a variable thickness-to-chord ratio (t/c) and 34° of nonlinear twist, while the steel spar blades have a constant t/c and no twist. The thickness and twist distributions for the aluminum blades are given in figures 2(a) and (b).

The Mod-0 wind turbine was operated with the highly twisted aluminum blades at nominal rotor speeds of 20 and 26 rpm. Due to slip of the fluid coupling in the drive train, actual rotor speeds were 21.0 and 27.4 rpm at the maximum powers

of 50 kW and 105 kW respectively. The blades remained fixed in pitch throughout these tests. Alternator output power and reference windspeed were recorded on magnetic tape and analyzed using the method of bins (ref. 6). A reference windspeed is measured by one of five hub height anemometers located in a semicircular array of 60 m radius around the wind turbine. The anemometer, which is most directly upwind, is chosen as the reference since it is believed to give windspeeds which are representative of the average freestream windspeed near the rotor.

Further tests were conducted using the steel spar blades with no twist. The rotor speed was 32 rpm. The inboard 70 percent of these blades remain fixed in pitch and thus experience high angles of attack at high windspeeds. As the wind speed increases, the wind turbine power output increases until the generator rating of 100 kW is reached. When wind speed increases further, it is necessary to pitch the outboard blade section so that the generator rating will not be exceeded. Since data from the anemometer array was not available at this time, a nacelle wind speed was used. The nacelle wind speed is measured by an anemometer located on the wind turbine nacelle.

## Baseline Performance Analysis Model

The Mod-0 rotors were modelled with the PROP Code. The aerodynamic characteristics used for the aluminum blade are given in figure 3 for a NACA 23018 "half-rough" airfoil. The characteristics shown in figure 3 are not measured data but instead were derived from a number of sources using some engineering judgment. The designation "half-rough" denotes aerodynamic data which are an average of NACA smooth and rough data given in reference 4. This roughness effect was included to account for manufacturing imperfections and for the accumulation of dirt as the airfoil is exposed to the environment.

Since the output of the PROP Code is rotor power with no drive-train losses, the following model based on experimental data was used to calculate the electrical power:

$$P_3 = -1.9 + 0.82 \quad P_2 \tag{1}$$

in which $P_3$ is the electrical power, (kW) and $P_2$ is the rotor power, (kW).

## Comparison of Measured and Predicted Performance (Baseline Model)

Figure 4 shows the predicted and measured power versus windspeed for the Mod-0 aluminum blades. The correlation between measured data and analysis using standard two-dimensional airfoil data is not very good. The obvious deficiencies of the predicted results are the less-than-measured maximum power and the rapid decrease in power after stall. The most interesting characteristic of the data is the relatively constant output power at high windspeeds for both rotor speeds. The leveling off of the power output occurs for wind speeds at which stall occurs over most of the blade. Maximum power is greater for the higher rotor speed since higher wind speed is required to achieve the same stall angle of attack. Results obtained for the Mod-0 steel spar blade are shown in figure 5. As shown in the data, the outboard section pitching continues to increase as wind speed increases. This data indicates a continuing production of torque by the inboard fixed-pitch portion of the blade, even though that section is stalled and producing negative power according to the model.

## Improved Performance Analysis Model

In an attempt to improve the correlation with experimental data, smooth airfoil characteristics were used. The fact that the baseline analysis underpredicted the actual performance suggested that the use of smooth airfoil data might improve correlation. By incorporating smooth airfoil characteristics, an increase in the maximum power resulted from the increased maximum lift and lower drag. Thus, it is recommended that smooth airfoil data be used to analyze wind turbine rotor performance near stall.

The use of smooth airfoil data, however, did not improve the rapid decrease in power after stall. Investigation of the airfoil characteristics reveals the reason for the predicted negative power at very high winds. Figure 6 shows an airfoil element operating with its chord line parallel to the plane of rotation, such as on the inboard portion of the steel spar rotor. The resultant wind velocity acts at an angle of attack, $\alpha$, with respect to the plane of rotation. The coefficients of lift, $C_L$, and drag, $C_D$, forces operating on the element can be resolved into a coefficient of torque force, $C_Q$, which acts in the plane of rotation. This coefficient is given by

$$C_Q = C_L \sin \alpha - C_D \cos \alpha \tag{2}$$

Using the baseline two dimensional airfoil data from figure 3 in equation (2) produces the torque coefficient characteristic shown in figure 7. This figure shows that negative torque can be expected for angles of attack between stall and 45°.

To improve the correlation between the measured and calculated performance after stall, an idealized stall model was used. This model was developed by deriving the airfoil characteristics in the stalled region that would produce performance similar to the measured data. The conditions placed on the model were threefold: (1) continuity of the stalled and unstalled characteristics at the stall angle, (2) constant power (or torque coefficient) after stall, and (3) the correct drag coefficient at 90° angle of attack for the given blade aspect ratio. The derivation of this model follows.

The torque force on a blade element is proportional to the coefficient of torque force and the square of the resultant velocity, or mathematically,

$$Q \sim C_Q V_R^2 \tag{3}$$

For a constant rotor speed we can divide by the constant $V_\Omega^2$, which yields

$$Q \sim C_Q \frac{V_R^2}{V_\Omega^2} \tag{4}$$

but from figure 6, $\cos \alpha = V_\Omega / V_R$, and thus

$$Q \sim \frac{C_Q}{\cos^2 \alpha} \tag{5}$$

Substituting Equation. (2) gives

$$Q \sim \frac{C_L \sin \alpha}{\cos^2 \alpha} - \frac{C_D}{\cos \alpha} \tag{6}$$

Two particularly convenient forms for the lift and drag characteristics after stall that satisfy the conditions stated above are given by

$$C_L = A_1 \sin 2\alpha + A_2 \frac{\cos^2 \alpha}{\sin \alpha} \tag{7}$$

and

$$C_D = B_1 \sin^2 \alpha + B_2 \cos \alpha \tag{8}$$

Substituting these into Equation (6) yields

$$Q \sim (2A_1 - B_1) \sin \alpha \tan \alpha + (A_2 - B_2) \tag{9}$$

Since the measured torque after stall is independent of wind speed it must also be independent of angle of attack. Thus, knowing that the derivative with respect to $\alpha$ must be zero, by inspection

$$A_1 = \frac{B_1}{2} \tag{10}$$

At an angle of attack of 90°, equation (8) gives

$$B_1 = C_{DMAX} \tag{11}$$

where $C_{DMAX}$ is the drag coefficient at $\alpha = 90°$.

For a finite aspect ratio blade

$$C_{DMAX} \simeq 1.11 + 0.18 AR \tag{12}$$

for $AR \leq 50$ based on experimental data from reference 7.

Thus

$$A = \frac{C_{DMAX}}{2} \tag{13}$$

Rearranging equation (7) and substituting equation (13) yields

$$A_2 = (C_L - C_{DMAX} \sin \alpha \cos \alpha) \frac{\sin \alpha}{\cos^2 \alpha} \tag{14}$$

Similarly equation (8) and (11) give

$$B_2 = \frac{C_D - C_{DMAX} \sin^2\alpha}{\cos \alpha} \tag{15}$$

For continuity with the below stall airfoil data, $A_2$ and $B_2$ are solved for the stall angle conditions, and thus equations (14) and (15) become

$$A_2 = (C_{Ls} - C_{DMAX} \sin \alpha_s \cos \alpha_s) \frac{\sin \alpha_s}{\cos^2 \alpha_s} \tag{16}$$

and

$$B_2 = C_{D_s} - \frac{C_{DMAX} \sin^2 \alpha_s}{\cos \alpha_s} \tag{17}$$

in which the subscript s denotes the value of the constant at stall.

The resulting airfoil characteristics for a NACA 23018 airfoil are given in figures 8 and 9 along with the standard two-dimensional airfoil data from figures 3 and 7.

### Comparison of Measured and Predicted Performance (Improved Model)

With these modifications to the airfoil characteristics, the predicted performance of the Mod-0 aluminum blade is found to correlate well with the measured data as shown in figure 10. Similar improvement was obtained for the Mod-0 steel spar blade as shown in figure 11. Since these two blades are significantly different in planform and twist, it is expected that this approach will produce satisfactory results for other configurations.

## HIGH TIP SPEED RATIO OPERATION

At high tip-speed ratios (low winds), a wind turbine may operate in the vortex ring state. Under this condition, the flow model developed by blade element-momentum theory breaks down. The induced axial interference factor, a, converges to values greater than 0.5. Since the flow far downstream would have twice the induced velocity, this suggests flow reversal, which is unlikely. In addition, empirical work by Glauert (ref. 3) has shown that the average rotor thrust coefficient differs greatly from the values calculated using momentum theory as shown in figure 12. The Glauert data may be used in the calculation of the local thrust coefficients. Wilson has suggested (ref. 8) that the following linear algebraic expression for the local thrust coefficient may be used:

$$C_T = 0.5775 + 0.96a \qquad a \leq 0.38 \tag{18}$$

The use of this empirical equation can eliminate convergence problems of the induced axial interference factor at high tip-speed ratios. Figure 13 shows a graphical representation of how the value of the interference factor is determined such that both momentum and blade element theories are satis-

fied. For a tip-speed ratio of 8, the two theories converge for a value of "a" of 0.37. At a tip-speed ratio of 12, however, no intersection occurs between the curves representing momentum and blade element theories. The use of the empirical curve, though, gives a converged solution at an "a" factor of 0.58.

Figure 14 shows measured power in low winds (high tip speed ratios) for the Mod-1 wind turbine described in table II. The Mod-1 is presented in this example since it is more likely to operate in the vortex ring state due to its high rotor solidity and high tip speed ratio. Theoretical power output using four methods is shown for comparison. The solid curve shows the results using the standard PROP code where the interference factor is limited to 1. This model tends to fall near the lower bound of the measured data. Limiting the interference factor to 0.5 has also been used since it prevents theoretical flow reversal in the far wake. However, as shown in figure 14, that model predicts power levels near the upper bound of the data. Limiting the interference factor to 0.7 or using the empirical curve gives results which more nearly represent the average of the data. For simplicity the interference factor was limited to 0.7 in the calculations of the next section.

## FURTHER COMPARISON OF THEORY WITH FIELD MACHINE DATA

For verification of the PROP code, comparisons were made with measured data from the Mod-0A and Mod-1 wind turbines. The Mod-0A and Mod-1 wind turbines are field machines which were designed to operate in an unattended mode. Engineering data is automatically recorded on magnetic tape. Ten-min averages of the power and wind speed are calculated using an energy method described in reference 9.

Figure 15 shows the measured and theoretical power output versus wind speed for the Mod-0A blades. The blade planform characteristics are given in table I(a) and figure 2. With the exception of at the rated wind speed (9.5 m/s), the measured data fall both above and below the theoretical curve. Near rated wind speed the data fall below the theoretical curve since the power is an average of times both below and at rated power. The mean power output density (power/rotor swept area) for the entire data set was 90 $W/m^2$. The theoretical mean power output density, however, was 89 $W/m^2$ for a mean deviation of +1 percent. Figure 16 shows the measured and theoretical power output for the Mod-1 60 m diameter steel blades described in table II. The measured data from this machine generally fall above the theoretical power output curve. The mean power output density for this data set was 250 $W/m^2$. The theoretical mean power output density, however, was 238 $W/m^2$ for a deviation of +5 percent.

## CONCLUSIONS

A method for calculating the output power from large horizontal axis wind turbines has been developed. This method is based on blade element-momentum theory with empirical modifications to the airfoil data and momentum theory. Smooth airfoil data is used for the unstalled operating region. Post-stall airfoil characteristics were derived to improve correlation with measured data, particularly at low tip-speed ratios. At high tip-speed ratios, empirical equations are used instead of momentum theory to calculate the values of the local thrust coefficients.

Output power calculated using the improved method were compared with data from several large wind turbines ranging in size from the 100 kW DOE/NASA Mod-0 (38-m rotor diam) to the 2000 kW Mod-1 (61-m rotor diam). The theoretical mean power densities are within 5 percent of the measured values for the cases examined.

## NOMENCLATURE

| | |
|---|---|
| a | axial interference factor, $a = (V_o - V_1)/V_o$ |
| AR | aspect ratio of blade, R/c, based chord length at 75 percent radius |
| $A_1$, $A_2$ | constants in lift coefficient equation after stall |
| $B_1$, $B_2$ | constants in drag coefficient equation after stall |
| B | number of blades |
| c | chord length, m |
| $C_D$ | drag force coefficient |
| $C_{Dmax}$ | drag force coefficient at 90° angle of attack |
| $C_L$ | lift force coefficient |
| $C_Q$ | torque force coefficient |
| $C_T$ | thrust force coefficient |
| $P_2$ | rotor output power, kW |
| $P_3$ | electrical output power, kW |
| Q | torque force, N |
| r | local radius, m |
| R | radius of rotor blade, m |
| $V_R$ | resultant velocity vector, m/s |
| $V_o$ | free-stream wind speed, m/s |
| $V_1$ | wind velocity at rotor plane, m/s |
| V | velocity due to rotation, m/s |
| $\alpha$ | angle of attack, deg |
| $\beta$ | blade twist angle, deg |
| s | value of airfoil characteristic at stall |

## REFERENCES

1. Wilson, R.E.; and Lissaman, P.B.S.: Applied Aerodynamics of Wind Power Machines. Oregon State University, July 1974. (NSF/RA/N-74-113, PB-238595/3.)

2. Jeng, D.R.; Keith, T.G.; and Aliakbarkhanafjeh, A.: Aerodynamic Performance Prediction of Horizontal Axis Wind Turbines. Wind Turbine Dynamics Conference. NASA CP-2185, DOE CONF-810226, pp. 9-18.

3. Glauert, H.: The Analysis of Experimental Results in the Windmill Brake and Vortex Ring States of an Airscrew. NASA RM-1026, Feb. 1926.

4. Abbott, I.H.; Von Doenhoff, A.E.; and Stivers, L.S.: Summary of Airfoil Data. NACA Rep. 824, 1945.

5. Critzos, C.C.; Heyson, H.H.; and Boswinkle, R.W.: Aerodynamic Characteristics of NACA 0012 Airfoil Section at Angles of Attack from $0^{o}$ to $180^{o}$. NACA TN-3361, 1955.

6. Richards, T.R.; and Neustadter, H.E.: DOE/NASA Mod-0A Wind Turbine Performance. DOE/NASA 1004-78/13, NASA TM-78916, 1978.

7. Hoerner, S.F.: Fluid Dynamic Drag. A. F. Hoerner, pub., 1965.

8. Wilson, R.E.: Aerodynamic Potpourri. Wind Turbine Dynamics Conference. NASA CP-2185, DOE CONF-801226, pp. 3-7.

9. Spera, D. A.; and Janetzke, D. C.: Performance and Load Data from the Mod-0A and Mod-1 Wind Turbine Generators. Presented at the Large Horizontal-Axis Wind Turbine Conference, (Cleveland, Oh.), July 1981.

TABLE I(a). - MOD-0/-0A ALUMINUM BLADE CHARACTERISTICS

| | |
|---|---|
| Rotor dia., m(ft) | 38.5 (126.4) |
| Number of blades | 2 |
| Root cutout, percent span | 5 |
| Pitch control (0/0A) | fixed/variable |
| Blade pitch 75% span, deg (0/0A +90 = Feather) | -2.8/0.0 |
| Airfoil | NACA 230 series |
| Taper | linear |
| Twist, deg | 34 (nonlinear) |
| Solidity | 0.031 |
| Precone, deg (0/0A) | 0.0/7.0 |
| Rotor shaft tilt, deg (0/0A) | 8.5/0.0 |

TABLE I(b). - MOD-0 STEEL SPAR BLADE CHARACTERISTICS

| | |
|---|---|
| Rotor dia., m(ft) | 38.4 (126.0) |
| Number of blades | 2 |
| Root cutout, percent span | 23 |
| Pitch control | 30 percent span tip control |
| Blade pitch inboard section, deg | 0 |
| Airfoil | NACA 23024 |
| Taper | linear |
| Solidity | .0.033 |
| Twist, deg | 0 |
| Precone, deg | 0 |
| Rotor shaft tilt, deg | 8.5 |

TABLE II. - MOD-1 BLADE CHARACTERISTICS

| | |
|---|---|
| Rotor dia., m(ft) | 61 (201.6) |
| Number of Blades | 2 |
| Root cutout, percent span. | 10 |
| Pitch control | variable |
| Blade pitch 75% span, deg (+90 = Feather) | 2 |
| Airfoil | NACA 44 series |
| Taper | linear |
| Twist, deg | 11 (linear) |
| Solidity | 0.043 |
| Precone, deg | 9 |
| Rotor shaft tilt, deg | 0 |

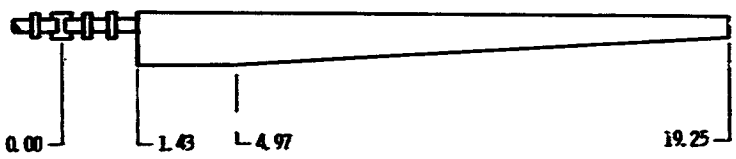


| RADIUS, m | CHORD, m |
|---|---|
| 1.43 | 1.473 |
| 4.97 | 1.473 |
| 19.25 | 0.457 |

(a)

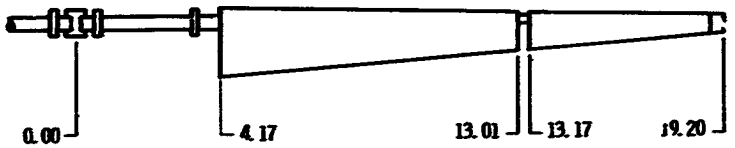


| RADIUS, m | CHORD, m |
|---|---|
| 4.17 | 1.964 |
| 13.01 | 1.171 |
| 13.17 | 1.154 |
| 19.20 | 0.672 |

(b)

(a) Aluminum.

(b) Steel.

Figure 1. - Mod-0/-0A blade planform.

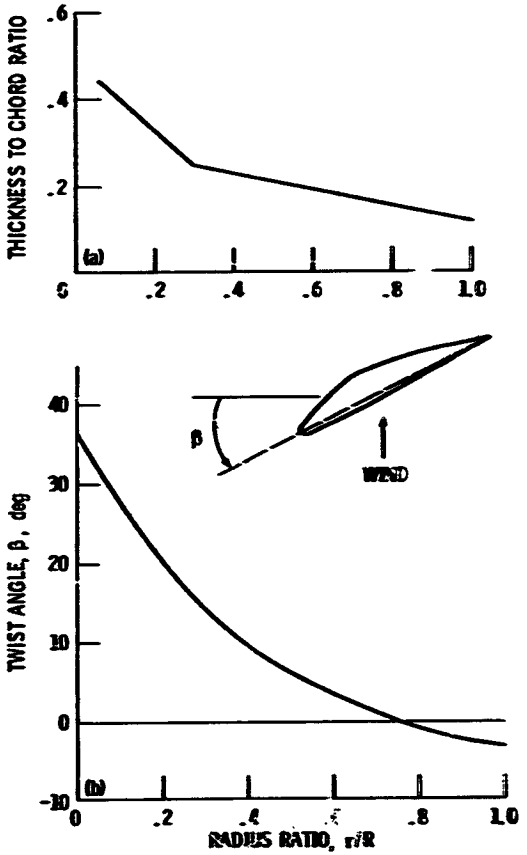


(a) - Aluminum blade thickness to chord ratio distribution.

(b) - Aluminum blade twist distribution.

Figure 2. - Aluminum blade characteristics.

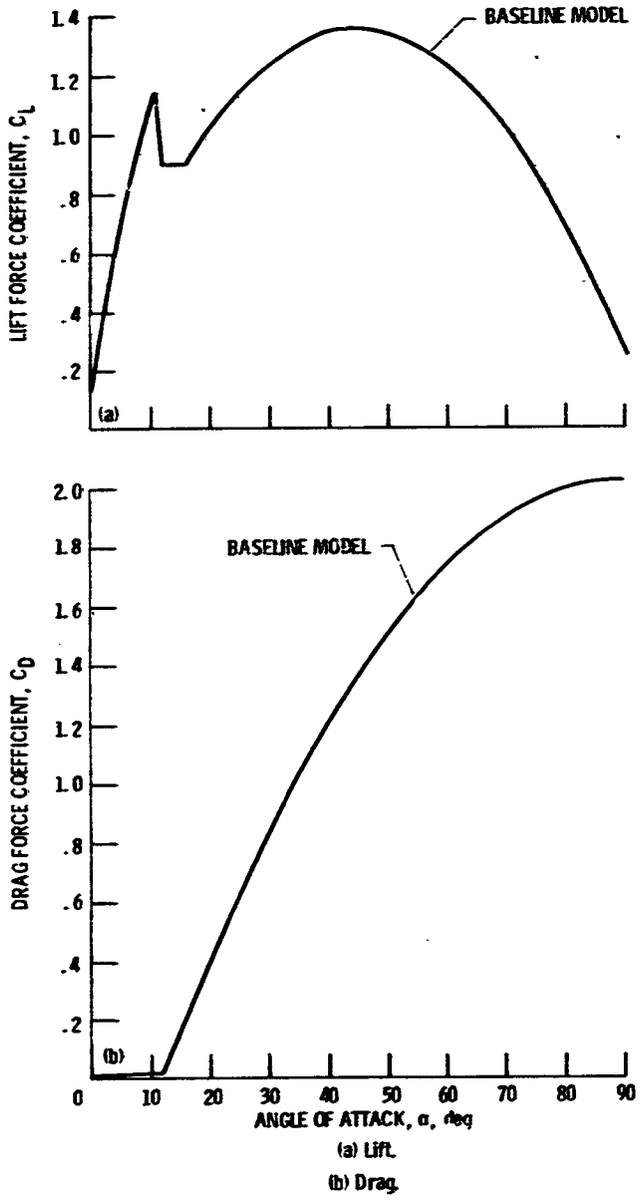


(a) Lift.

(b) Drag.

Figure 3. - Synthesized aerodynamic data for "half-rough" NACA 23018 airfoil used in the baseline model.

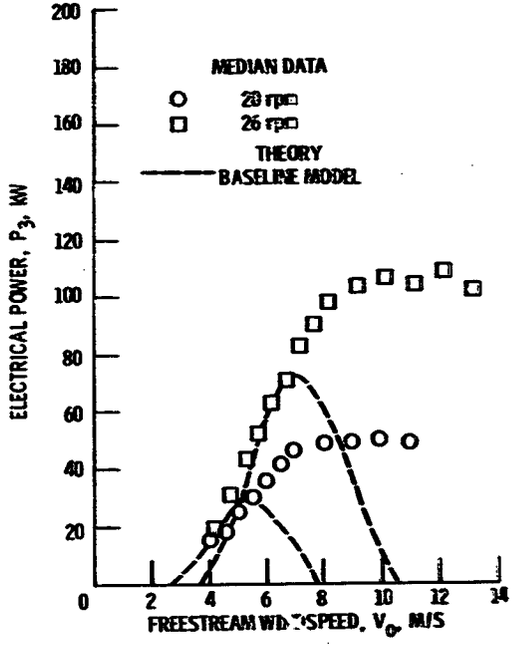


Figure 4. - Comparison of measured and calculated performance using baseline model for the Mod-0 aluminum blades at fixed pitch.

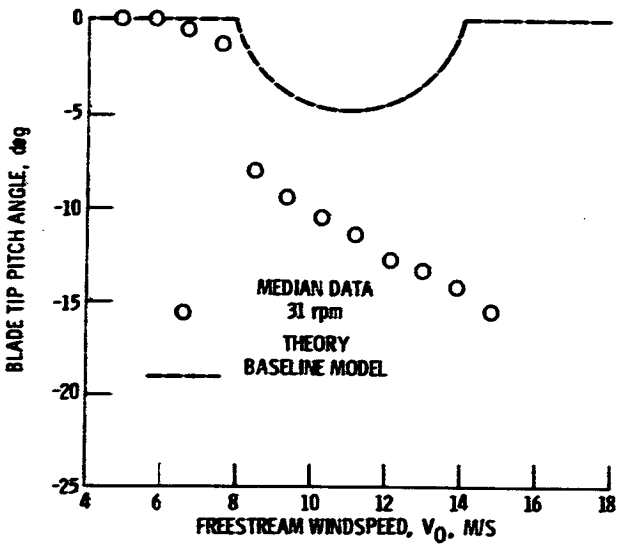


Figure 5. - Comparison of measured and calculated tip angle versus windspeed using baseline model for the Mod-0 steel spar, tip control blades.

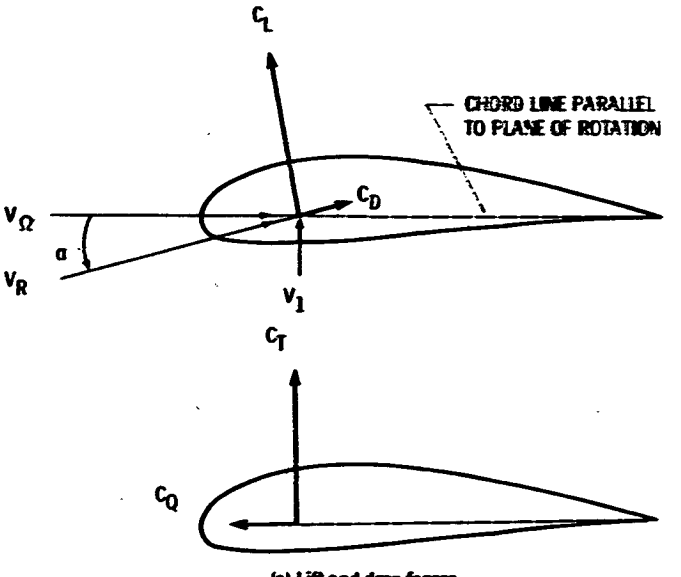


(a) Lift and drag forces
(b) Thrust and torque forces

Figure 6. - Blade element wind velocity and force vector diagrams.

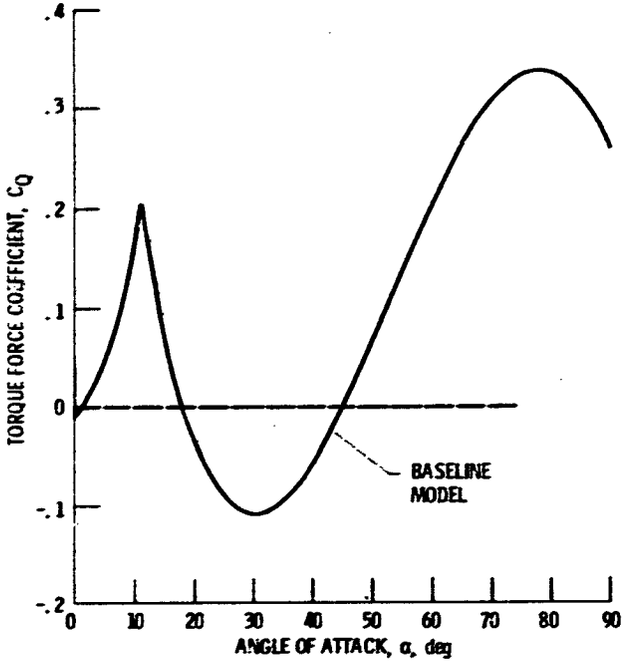


Figure 7. - Aerodynamic torque force coefficient versus angle of attack for "half-rough" NACA 2301B airfoil used in the baseline model.

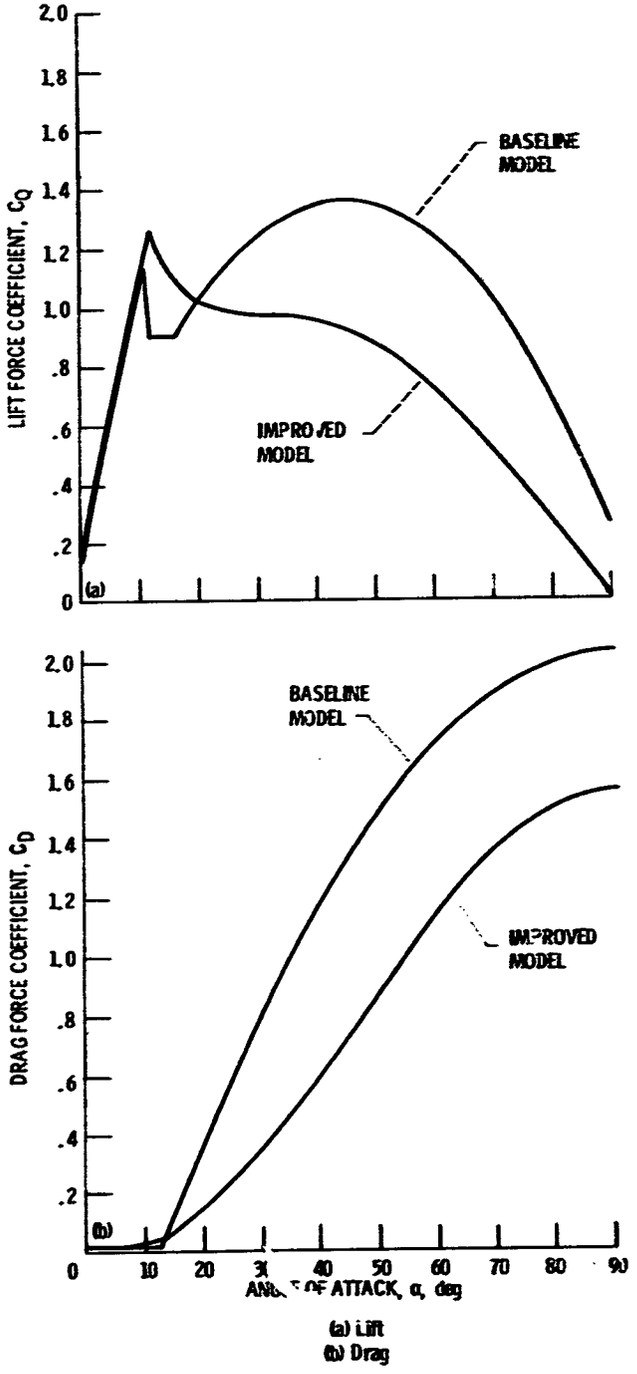


(a) Lift
(b) Drag

Figure 8. - Comparison of the NACA 2301B airfoil data for the baseline and the improved aerodynamic models.

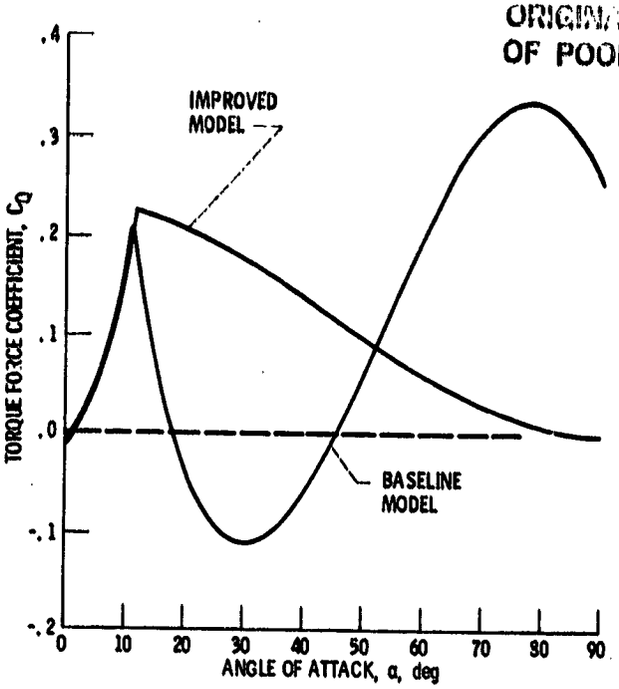


Figure 9. - Comparison of torque coefficients for the baseline and the improved aerodynamic models.

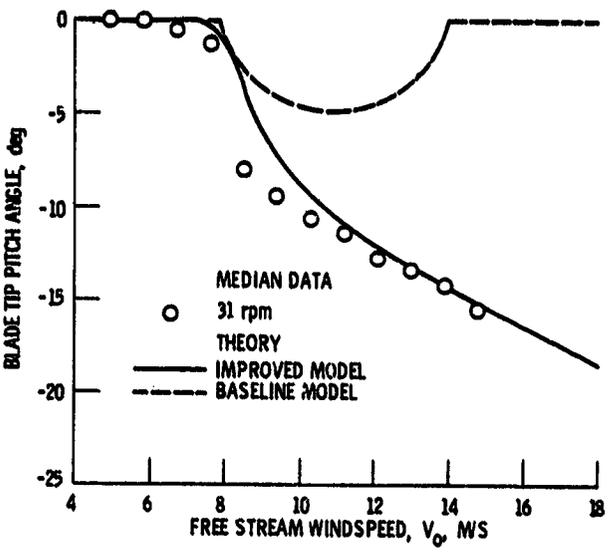


Figure 11. - Comparison of measured and calculated tip angle versus windspeed for the Mod-0 steel spar tip control blades.

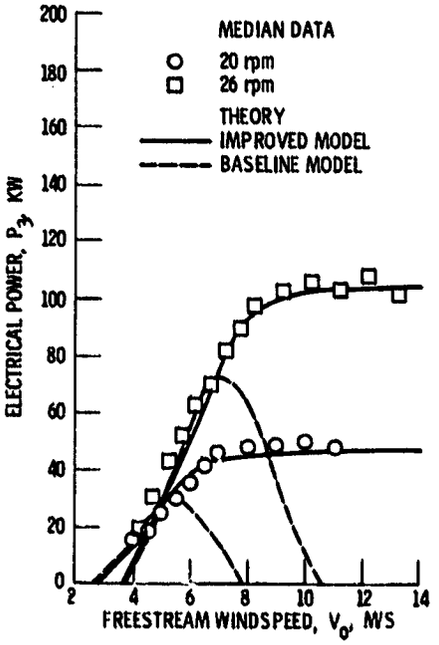


Figure 10. - Comparison of measured and calculated performance for the Mod-0 aluminum blades.

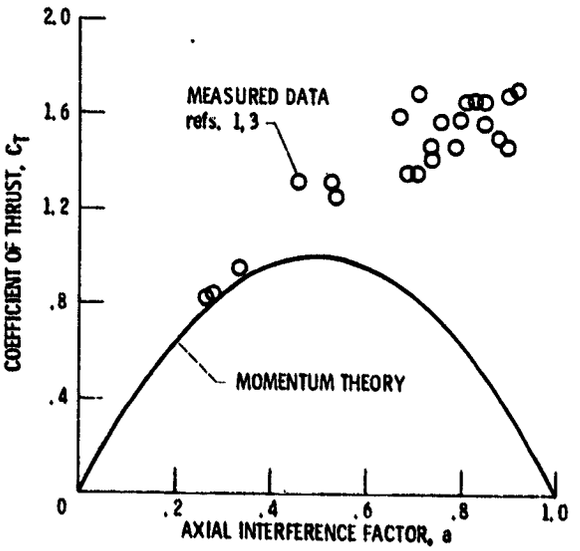


Figure 12. - Comparison of theoretical and measured rotor thrust force coefficients.

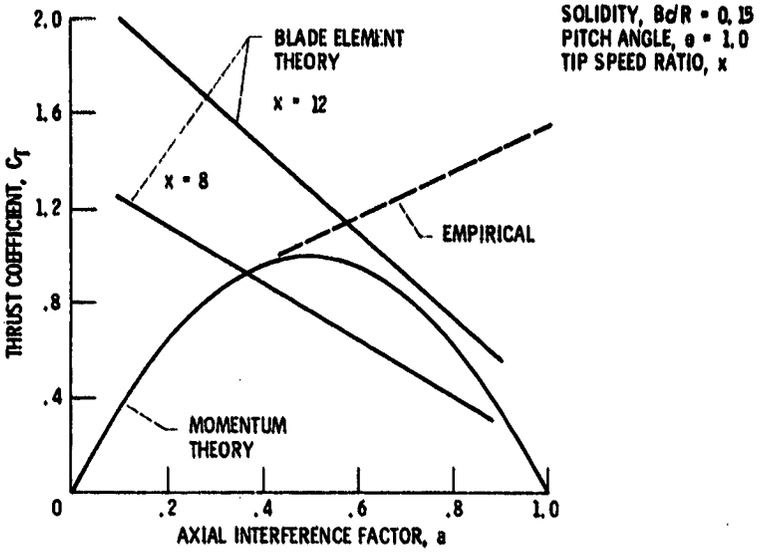


Figure 13. - Theoretical and empirical rotor thrust force coefficients.

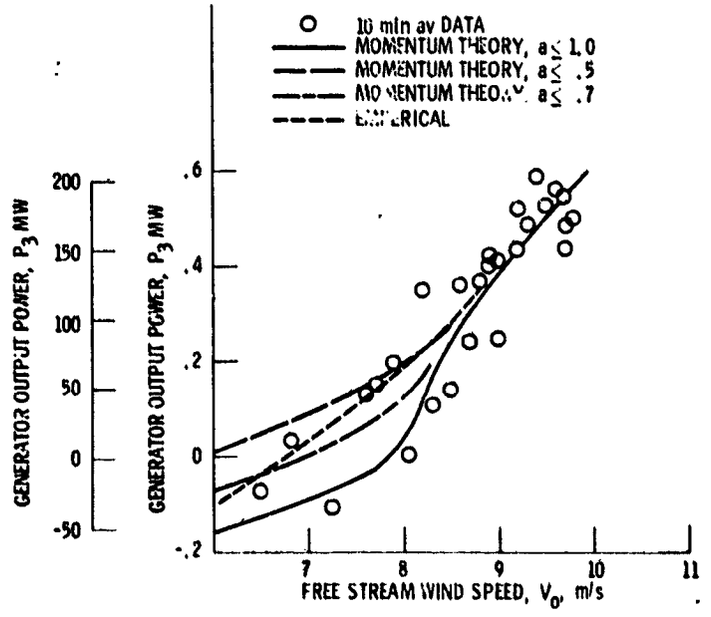


Figure 14. - Experimental and theoretical output power from the Mod-1 wind energy system.

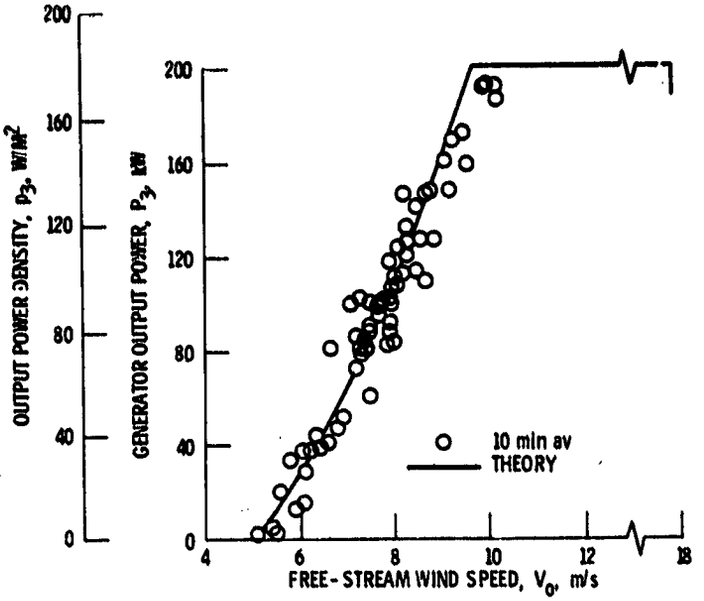


Figure 15. - Output power from the Mod-0A 200 kW wind energy system operating at 40 rpm with aluminum blades.

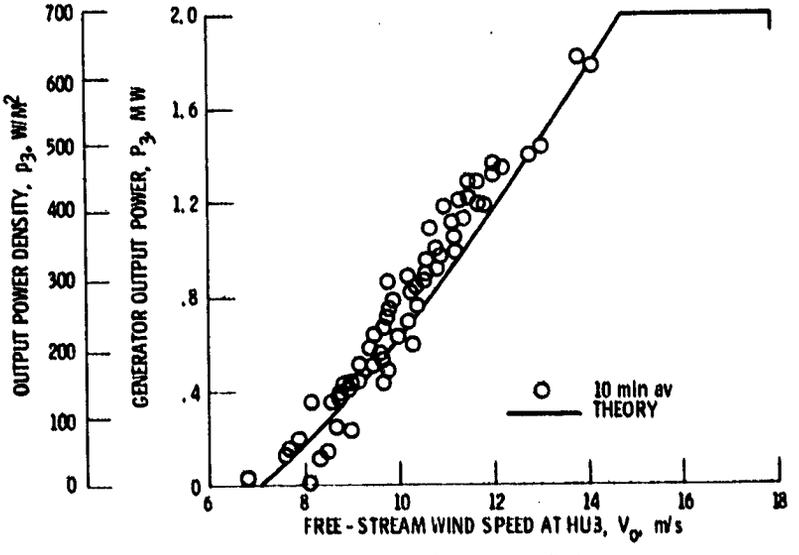


Figure 16. - Output power from the Mod-1 2000 kW wind energy system.